

Pulsed-microwave-induced thermoacoustic tomography: Filtered backprojection in a circular measurement configuration

Minghua Xu and Lihong V. Wang^{a)}

Optical Imaging Laboratory, Biomedical Engineering Program, Texas A&M University, 3120 TAMU, College Station, Texas 77843-3120

(Received 12 December 2001; accepted for publication 7 May 2002; published 16 July 2002)

Our study on pulsed-microwave-induced thermoacoustic tomography in biological tissues is presented. A filtered backprojection algorithm based on rigorous theory is used to reconstruct the cross-sectional image from a thermoacoustic measurement in a circular configuration that encloses the sample under study. Specific details describing the measurement of thermoacoustic waves and the implementation of the reconstruction algorithm are discussed. A two-dimensional (2D) phantom sample with 2 mm features can be imaged faithfully. Through numerical simulation, the full width half-maximum (FWHM) of the point-spread function (PSF) is calculated to estimate the spatial resolution. The results demonstrate that the circular measurement configuration combined with the filtered backprojection method is a promising technique for detecting small tumors buried in biological tissues by utilizing microwave absorption contrast and ultrasound spatial resolution (\sim mm).
© 2002 American Association of Physicists in Medicine. [DOI: 10.1118/1.1493778]

Key words: microwave, thermoacoustics, tomography, imaging, filtered backprojection

I. INTRODUCTION

Pulsed microwave-induced thermoacoustic tomography combines the advantages of both ultrasound spatial resolution and microwave absorption contrast.¹⁻⁴ The basic idea of this technique is that a very short microwave pulse ($<1 \mu\text{s}$) heats a sample; the sample then absorbs the microwave energy and simultaneously generates temporal thermoacoustic waves, which are strongly related to the locally absorbed microwave energy. The microwave pulse is so short that the heat diffusion's effect on the thermoacoustic wave can be ignored. The thermoacoustic signals have a wide frequency range up to MHz and carry the information of the microwave absorption distribution with millimeter spatial resolution. In practice, microwaves at 300 MHz–3 GHz with 0.1–1 μs pulse are often adopted, which offer penetration depths of several centimeters in biological tissues. For example, the penetration depths for fat and muscle tissues at 3 GHz microwaves are 9 and 1.2 cm, respectively.³ Most other soft tissues have penetration depths in between those for muscle and fat tissues. The wide range of values among various tissues makes it possible to achieve high image contrast. In addition, the long penetration depth allows this technique to detect interior tumors.

In our initial studies, we used focused transducers with big apertures to detect thermoacoustic signals with both the linear scan^{2,3} and the circular scan methods.⁴ The big aperture gives us a good signal-to-noise ratio (SNR), because the SNR is inversely proportional to the square root of the aperture area. Each scan line is converted into a one-dimensional image along the axis of the transducer, and then cross-sectional images can be obtained by straightforward calculations. The axial resolution is obtained by measuring the temporal profiles of the thermoacoustic signals. However, the lateral resolution is mainly determined by the focal diameter

of the transducer.^{2,5} The image view is also limited by the focal length of the transducer.

An alternative method is to use unfocused transducers with small apertures to record the thermoacoustic signals and then reconstruct the microwave absorption distribution from the measured data. The different measurement configuration may, however, result in a different reconstruction algorithm. Under certain practical conditions, on a rigorous base, we theoretically reported a modified backprojection method for the planar, cylindrical, and spherical recording configurations.^{6,7} These were computed through temporal spatial backprojection and coherent summation over spherical surfaces with spatial weighting factors. This method is something like synthetic aperture. Therefore, the SNR can be greatly improved through coherent summation, although the SNR of each detected temporal signal may be reduced due to the small aperture of the unfocused transducer as compared to focused transducers with big apertures.

In this paper, we present our study on pulsed-microwave-induced thermoacoustic tomography in biological tissues under a circular measurement configuration. A wide beam ($\sim 22 \text{ cm}^2$) of short-pulse (0.5 μs) microwave energy is used to illuminate a sample from the bottom. The sample absorbs the microwave energy and generates temporal thermoacoustic waves simultaneously. An unfocused ultrasonic transducer with a small aperture (6 mm) is used to record the thermoacoustic signals. A filtered backprojection (FBP) method based on rigorous theory is used to reconstruct the cross-sectional image from the measured data. Specific details describing the measurement of thermoacoustic waves and the implementation of the reconstruction algorithm are discussed. A phantom sample is investigated. The reconstructed image agrees with the original sample very well. Through

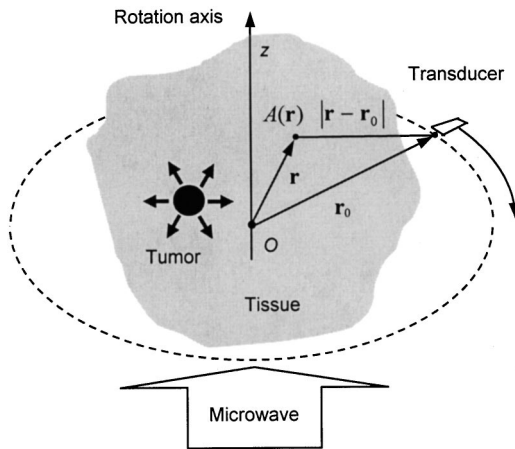


FIG. 1. Scheme of thermoacoustic circular measurement. Microwave pulses are transmitted to the sample from the bottom. The tumor inside absorbs the energy and generates thermoacoustic waves. An ultrasonic transducer at position r_0 records the thermoacoustic signals.

numerical calculation of the point-spread function, the spatial resolution is estimated to reach \sim mm.

II. METHOD OF MEASUREMENT

There are three typical measurement geometries: linear or planar configuration, circular or cylindrical configuration, and spherical configuration. The choice of measurement geometry depends on the practical need. For the purposes of investigating external organs, the second two choices are preferred. In practice, at least two restraints should be considered. One is that the space for delivering microwaves to the sample is physically limited. Ideally, the sample should be homogeneously illuminated as much as possible. Otherwise, the thermoacoustic signal will reflect not only the absorption differentiation, but also inhomogeneous illumination, which will result in reconstruction artifacts. The other restraint is that it is physically impossible to collect measurements over a 4π solid angular range. The developed reconstruction algorithm requires that the detectors receive outgoing thermoacoustic waves from all possible angular directions.^{6,7} But, in reality, a limited angular range has to be tolerated, and the incomplete data also results in some reconstruction artifacts.

In this study, we chose a circular measurement configuration, as shown in Fig. 1. Tissue, such as breast tissue, is hard to compress but easy to deform. A slight force can make the external tissue nearly cylindrical in shape. Then, the microwave can be delivered to the tissue from its larger bottom and the detector can measure the outgoing thermoacoustic waves in a circular geometry around the tissue. The wavelength of microwaves below 3 GHz is relatively long, e.g., at 3 GHz, 10 cm in air, and 3 cm in soft tissue, compared to the typical size of tissue investigated in several centimeters diameter. That helps to illuminate the tissue homogeneously. However, because of attenuation, microwaves along the z axis decay exponentially and the generated thermoacoustic signal along the z axis decays exponentially, too, even in a

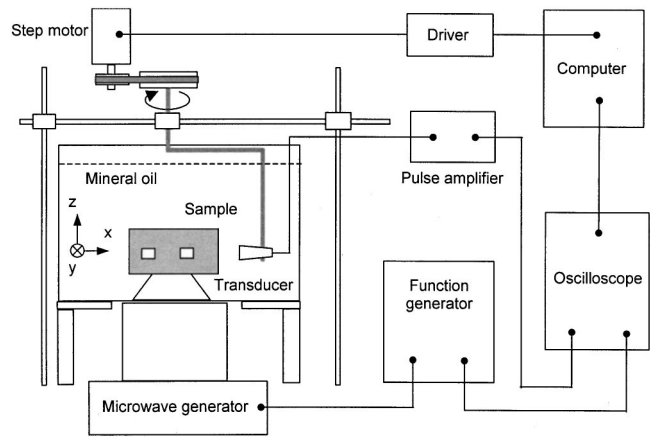


FIG. 2. Experimental setup.

homogenous sample. But the circular detection plane, i.e., the horizontal xy plane, is parallel with the incident plane of microwave pulses. Besides, due to the bounded water and salt in cancer cells,^{8,9} the tumor will absorb more microwave energy and generate more intense thermoacoustic waves than the surrounding tissue. Therefore, the thermoacoustic signals from the circular plane have a significantly reduced dynamic range compared with those in any other planes. This improves the accuracy of both data acquisition and data reconstruction tremendously. As shown below, reasonable reconstruction images are achieved in the experiment.

Figure 2 shows the experimental setup we used for the circular measurement configuration. A Plexiglas container is filled with mineral oil. An unfocused transducer is immersed inside it and fixed on a rotation device. A step motor drives the rotation device and then moves the transducer scan around the sample on a horizontal x - y plane, where the transducer horizontally points to the rotation center. A sample is immersed inside the container and placed on a holder: it is made of a thin plastic material, which is transparent to microwaves. The transducer (V323, Panametrics) has a central frequency of 2.25 MHz and a diameter of 6 mm.

The microwave pulses transmitted from a 3 GHz microwave generator have a pulse energy of 10 mJ and a pulse width of $0.5 \mu\text{s}$. A function generator (Protek, B-180) is used to trigger the microwave generator, control its pulse repetition frequency, and synchronize the oscilloscope sampling. In our experiments, the pulse repetition frequency is 50 Hz and the oscilloscope sampling frequency is 20 MHz. Microwave energy is delivered to the sample by a rectangular waveguide with a cross section of $72 \text{ mm} \times 34 \text{ mm}$. A personal computer is used to control the steps. The signal from the transducer is first amplified through a pulse amplifier, then recorded and averaged 500 times by an oscilloscope (TDS640A, Tektronix), and finally transferred to a personal computer for imaging.

This system is within the IEEE standard for safety levels with respect to human exposure to radio frequency electromagnetic fields (see the Appendix). The waveguide is filled with air and has a mode of $\text{TE}_{1,0}$. The wavelength of the

emitted microwave is 10 cm in air. The microwave irradiates from the waveguide and then propagates through a thin layer of air into the container and the tissue sample. Due to the relatively long wavelength of microwave in tissue (~3 cm at 3 GHz), the diffraction causes only smooth variations on a scale comparable to 3 cm. As discussed later, in signal processing, we removed the low-frequency component below 50 KHz, which corresponds to an acoustic wavelength of ~3 cm. Therefore, the effect of mode structure of microwave irradiation on thermoacoustic imaging is minor.

III. METHOD OF RECONSTRUCTION

We assume a tissue with inhomogeneous microwave absorption but a relatively homogeneous acoustic property. When the microwave pulse duration is <1 μs, the heat diffusion's effect on the thermoacoustic wave in the tissue can be ignored. The speed of sound in most soft tissue is relatively constant at ~1.5 mm/μs. Therefore, the pressure $p(\mathbf{r}, t)$ produced by the heat source $H(\mathbf{r}, t)$ obeys the following equation:¹⁰

$$c^2 \nabla^2 p(\mathbf{r}, t) - \frac{\partial^2}{\partial t^2} p(\mathbf{r}, t) = -\Gamma(\mathbf{r}) \frac{\partial H(\mathbf{r}, t)}{\partial t}, \quad (1)$$

where the Grüneisen parameter $\Gamma(\mathbf{r}) = \beta c^2 / C_p$, c is the speed of sound; β is the isobaric volume expansion coefficient; C_p is the heat capacity; and $H(\mathbf{r}, t)$ is the heating function defined as the thermal energy per unit time and unit volume deposited by the energy source. Basically, the heating function can be written as the product of a spatial absorption function and a temporal illumination function:

$$H(\mathbf{r}, t) = A(\mathbf{r})I(t). \quad (2)$$

Suppose a delta illuminating function $\delta(t)$, the detected acoustic pressure $p(\mathbf{r}_0, t)$ on the circular surface $\mathbf{r} = \mathbf{r}_0 = (\rho_0, \varphi_0, z_0)$, and time t can be written as⁶

$$p(\mathbf{r}_0, t) = \frac{1}{c} \frac{\partial}{\partial t} \int \int \int d^3r D(\mathbf{r}) \frac{\delta(ct - |\mathbf{r}_0 - \mathbf{r}|)}{4\pi|\mathbf{r}_0 - \mathbf{r}|}, \quad (3)$$

where $D(\mathbf{r}) = A(\mathbf{r})\Gamma(\mathbf{r})$. The inverse problem is to reconstruct the spatial distribution $D(\mathbf{r})$ from a set of data $p(\mathbf{r}_0, t)$ measured at a different position \mathbf{r}_0 .

Due to the finite bandwidths of the transducer, the pre-amplifier and the microwave pulse, only a portion of the information about the absorption structure can be restored. The high-frequency component of the thermoacoustic signal primarily reflects the small size structure while the low-frequency component primarily reflects the large size structure. If challenged to detect small size tumors, we can safely remove the low-frequency component. Besides, the wavelengths of the high-frequency thermoacoustic waves are much smaller than the detecting distance between the thermoacoustic source and the transducer. Under the above conditions, i.e., $\rho_0 k \gg 1$ or $k|\mathbf{r} - \mathbf{r}_0| \gg 1$, where k is the wave number, we have shown theoretically that the distribution $D(\mathbf{r})$ can be calculated by the following 2D surface integral in the cylindrical configuration:⁷

$$D(\rho, \varphi, z) = -\frac{1}{2\pi c^2} \int \int_{S_0} dS_0 [\mathbf{n} \cdot \mathbf{n}_0] \frac{1}{t} \frac{\partial p(\mathbf{r}_0, t)}{\partial t} \Big|_{t=|\mathbf{r}-\mathbf{r}_0|/c}, \quad (4)$$

where

$$\begin{aligned} \mathbf{n} \cdot \mathbf{n}_0 &= \frac{|\boldsymbol{\rho} - \boldsymbol{\rho}_0|}{|\mathbf{r} - \mathbf{r}_0|} = \sqrt{\frac{\rho^2 + \rho_0^2 - 2\rho\rho_0 \cos(\varphi_0 - \varphi)}{|\mathbf{r} - \mathbf{r}_0|^2}} \\ &= \sqrt{1 - \frac{(z_0 - z)^2}{|\mathbf{r} - \mathbf{r}_0|^2}}, \end{aligned} \quad (5)$$

$dS_0 = \rho_0 d\varphi_0 dz_0$, $\boldsymbol{\rho}$ and $\boldsymbol{\rho}_0$ are the projections of \mathbf{r} and \mathbf{r}_0 on the z plane, respectively, and \mathbf{n} and \mathbf{n}_0 are unit vectors pointing along the line joining $\boldsymbol{\rho}$ and $\boldsymbol{\rho}_0$ and along the line joining \mathbf{r} and \mathbf{r}_0 , respectively. This is a modified backprojection formula of quantity $-(1/t)[\partial p(\mathbf{r}_0, t)/\partial t]$. The weighting factor $[\mathbf{n} \cdot \mathbf{n}_0]$ is less than 1, except if $z = z_0$, $[\mathbf{n} \cdot \mathbf{n}_0] = 1$. That indicates that the cross-sectional image of any z_0 plane is mainly determined by the data measured on the circle of the same z_0 plane. In other words, if some small absorption sources are located on a z_0 plane, a set of circular measurement data on the same plane would be sufficient to yield a good cross-sectional image.

The quantity $\partial p(\mathbf{r}_0, t)/\partial t$ can be calculated through the Fourier transform,

$$\frac{\partial p(\mathbf{r}_0, t)}{\partial t} = \text{FFT}^{-1}\{-i\omega p(\mathbf{r}_0, \omega)W_\Omega(\omega)\}, \quad (6)$$

where FFT^{-1} denotes the fast inverse Fourier transform; ω is angular frequency and equal to $2\pi f$; $W_\Omega(\omega)$ is a window function; and the Fourier transform defines

$$\bullet(\omega) = \int_{-\infty}^{+\infty} \bullet(t)\exp(i\omega t)dt. \quad (7)$$

We want to point out that the factor ω in Eq. (6) actually represents a pure ramp filter, which will significantly depress the low-frequency signal. That is helpful to guarantee the validity of the reconstruction, Eq. (4). The ramp filter can also amplify the high-frequency noise in such a way that the reconstructed image is not acceptable from the physical point of view. In order to avoid this effect, it is necessary to introduce a relative low-pass filter $W_\Omega(\omega)$ characterized by a cutoff angular frequency $\Omega = 2\pi f_\Omega$. A Hanning window is our choice in this case:

$$W_\Omega(\omega) = \begin{cases} 0.5 + 0.5 \cos\left(\pi \frac{\omega}{\Omega}\right), & \text{if } |\omega| < \Omega, \\ 0, & \text{otherwise.} \end{cases} \quad (8)$$

Thus, the reconstruction algorithm can also be termed a filtered backprojection (FBP) with the modified ramp filter $\omega W_\Omega(\omega)$. Unlike the FBP algorithm used in x-ray tomography,¹¹ which uses surface integration over intersecting planes, the method in our problem is calculated through temporal backprojection and coherent summation over spherical surfaces with a certain spatial weighting factor.

IV. EXPERIMENT

The experimental conditions necessitate special care. The reconstruction theory requires point detectors, and the real transducer must never be a point. But, we can ignore its size if we put it at a distance from the sample that is greater than the size of the transducer aperture. In addition, we must shield both the transducer and the electrical transmission cables from microwave illumination. Otherwise, the microwave pumping will cause harmful electrical signals via electromagnetic induction. If well shielded, the induced signal decays very rapidly. A time gate can cut out the induced signal before the arrival of the thermoacoustic signal. Suppose $p(\mathbf{r}_0, t)$ is the thermoacoustic signal with delta-pulse microwave pumping, then the measured thermoacoustic signal can be written as a convolution with the measurement system response $H(t)$:

$$S(\mathbf{r}_0, t) = p(\mathbf{r}_0, t) * H(t). \tag{9}$$

Considering the temporal response $M(t)$ of the amplifier, the impulse response $R(t)$ of the transducer and the temporal profile $I(t)$ of the microwave pulse, $H(t)$ can also be written as a convolution,

$$H(t) = M(t) * I(t) * R(t). \tag{10}$$

In the frequency domain, Eq. (9) can be written as

$$S(\mathbf{r}_0, \omega) = p(\mathbf{r}_0, \omega) H(\omega). \tag{11}$$

Basically, we cannot recover all of the available information because of the limited bandwidth of the detection system. The information we can acquire depends on the system response $H(\omega)$. In practice, $M(\omega)$ is very wide and ~ 1 ; $I(\omega)$ determines the bandwidth of the generated thermoacoustic signal, which is approximately inversely proportional to the width of its temporal profile; $R(\omega)$ is a wide-band transducer with a central frequency ω_c . If $H(\omega)$ is known, an appropriate deconvolution algorithm can be used to figure out $p(\mathbf{r}_0, \omega)$.

In our experiments, the illumination $I(t)$ is approximately a rectangular function with duration $\tau = 0.5 \mu\text{s}$, and its temporal profile is shown as the short dashed line in Fig. 3(a), which determines the frequency of the generated thermoacoustic signal below 2 MHz. The transducer that we used is of the videSCAN type with a central frequency of $f_c = 2.25 \text{ MHz}$, and its temporal profile is shown as the solid line in Fig. 3(a). In the frequency range below 2 MHz, the response of the transducer approximates a ramp filter. As shown in Fig. 3(b), the calculated $H(f)$ (solid line) was compared with a pure ramp filter f (short dashed line). In this special case for our measurement system, the filtered $\partial p(\mathbf{r}_0, t) / \partial t$ can be approximately calculated by an inverse Fourier transformation as

$$\frac{\partial p(\mathbf{r}_0, t)}{\partial t} \approx \text{FFT}^{-1}\{S(\mathbf{r}_0, \omega) W_\Omega(\omega)\}. \tag{12}$$

Next, we imaged a phantom sample with a complex absorption structure using the following procedure. First, we used screwdrivers to carve a structure: the word ‘‘OIL’’ (ab-

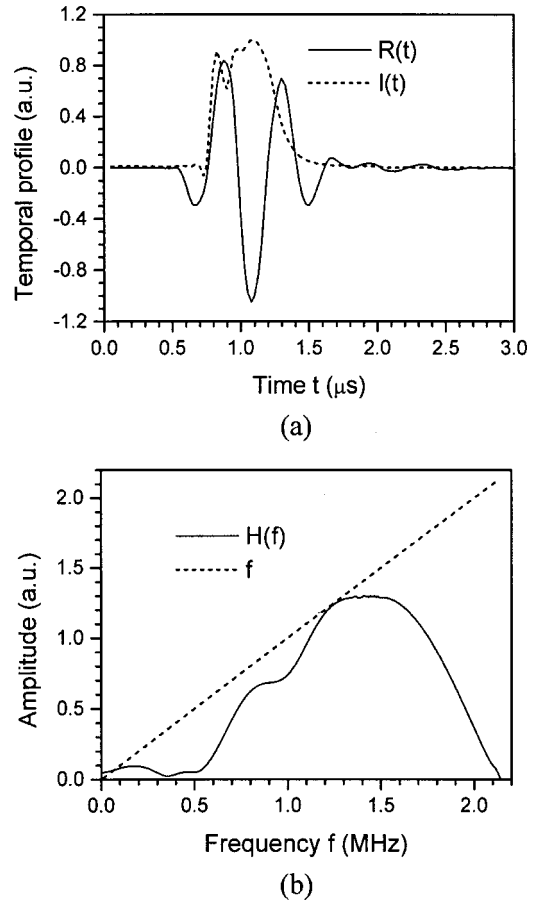


Fig. 3. (a) The impulse response of the transducer $R(t)$ and the temporal profile of the microwave pulse $I(t)$; (b) the system response $H(f)$ and the pure ramp filter f .

brexiation for Optical Imaging Lab) in a large fat base. The diameter of the dent was about 2 mm. In the meantime, we prepared a hot solution with 5% gelatin, 1% salt, and a drop of dark ink to improve the photographic properties. Then we used an injector to inject several drops of the hot solution into the dents and subsequently blew out the air to assure good coupling between the gelatin solution and the fat tissue. The gelatin word was cooled at room temperature until solidified. The photograph of the sample at this stage is shown in Fig. 4(a). Finally, we added a piece of fat both on the top and on the bottom of the sample so that the gelatin word was buried inside the fat tissue. The diagram of the structure in side view is shown in Fig. 4(b).

The transducer rotationally scanned the sample from 0° – 360° with step size 2.25° in the plane, including the word ‘‘OIL.’’ The distance between the transducer and the rotation center was 8 cm. The sampling frequency of the oscilloscope was 20 MHz. We chose the cutoff frequency $f_\Omega = 4 \text{ MHz}$ in the filter W_Ω . The filtered temporal thermoacoustic signals are shown in Fig. 4(c). Because of some time delay in the oscilloscope, the rotation origin is at time $t = 36.8 \mu\text{s}$. Unlike X-ray tomography,¹¹ these data have no symmetric property in a 2π period. The reconstructed image produced by our filtered backprojection method, which agrees with the original sample very well, is shown in Fig. 4(d). However, when

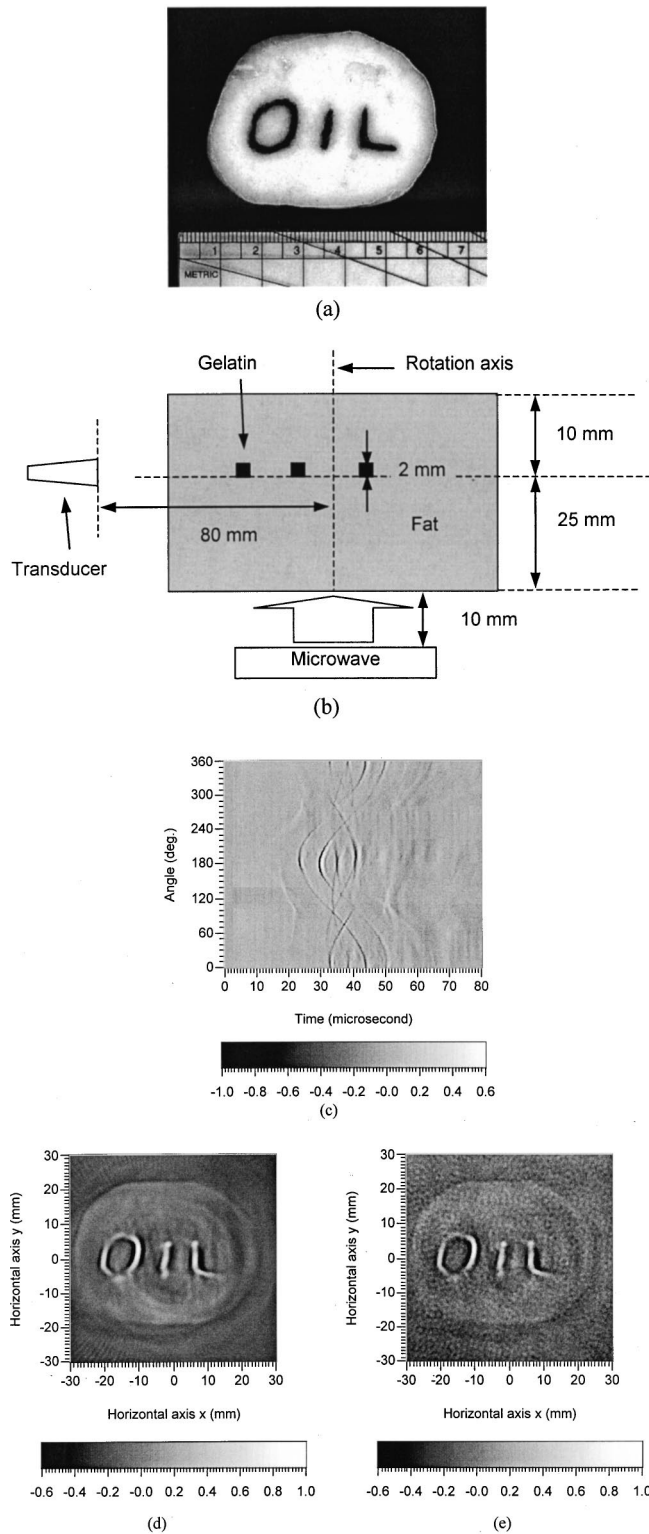


FIG. 4. (a) Cross-sectional photograph of the sample; (b) the diagram of the measurement in side view; (c) the filtered thermoacoustic temporal signals detected at different angular positions from 0°–360°; (d) the reconstructed image with filtering; (e) the reconstructed image without filtering.

the filter W_{Ω} was not used to depress the high-frequency noise, the reconstructed image displayed certain randomly distributed spots, as shown in Fig. 4(e), which degrade the image quality a lot.

In signal processing, we removed only the low-frequency component below 50 KHz. As shown in Fig. 4(d), the boundary and location of the large fat base with a 5 cm diameter was also faithfully imaged. Therefore, we conclude that the removal of low frequencies in signal processing will not have much effect on the detection of relatively large structures. The location and boundary of the microwave absorption structures are primarily determined by the relatively high-frequency component of the thermoacoustic signals.

V. NUMERICAL SIMULATION

The full width half-maximum (FWHM) of the point-spread-function (PSF) profile can be used to represent the spatial resolution.¹² Through numerical simulation, we can calculate the PSF profiles and then estimate the spatial resolution.

The limit band of the detection system is a primary factor in limiting the spatial resolution. Consider a point source at axis $x = x_p$, which can be written in the circular polar coordinates as

$$D(\mathbf{r}_p) = \frac{\delta(\rho - x_p) \delta(\varphi) \delta(z)}{\rho} \tag{13}$$

Substituting it into Eq. (3), and taking the Fourier transform, it is easy to obtain the generated thermoacoustic wave in the frequency domain,

$$p(\mathbf{r}_0, \omega) = \frac{-i\omega \exp(ikd)}{4\pi c^2 d} \tag{14}$$

where d is the distance between the point source and the detector,

$$d = \sqrt{\rho_0^2 + x_p^2 - 2\rho_0 x_p \cos \varphi_0 + z_0^2} \tag{15}$$

For simplicity, we only consider a circular measurement in the plane $z_0 = 0$. We assume the sampling frequency is 20 MHz and use the Hanning window to simulate the limit band of the detection system. Figure 5(a) shows three examples of ramp filters modified by Hanning windows with cutoff frequencies at 4, 2, and 1 MHz, respectively. We use Eq. (6) to calculate derivatives of the temporal thermoacoustic signals. Finally, the FBP, Eq. (4), is employed to reconstruct images from the simulated data.

The numerical calculations demonstrate that the PSF is radially symmetric only when the point source is located at the origin. Such examples of PSF radial profiles with different cutoff frequencies are shown in Fig. 5(b). When a point source is off center, the PSF is not radially symmetric. Figure 5(c) shows some examples of PSF radial profiles when the point source is at $x_p = 30$ mm. The farther the point is off the origin, the more distortion the PSF has. But the distortion is not significant and the PSF does not expand in either the lateral or axial direction by very much. Therefore, the PSF and FWHM can be regarded as nearly space invariant. Of course, if the detector system has a lower cutoff frequency, the width of the PSF profile has more extension and the spatial resolution becomes lower. Only a wide band signal at

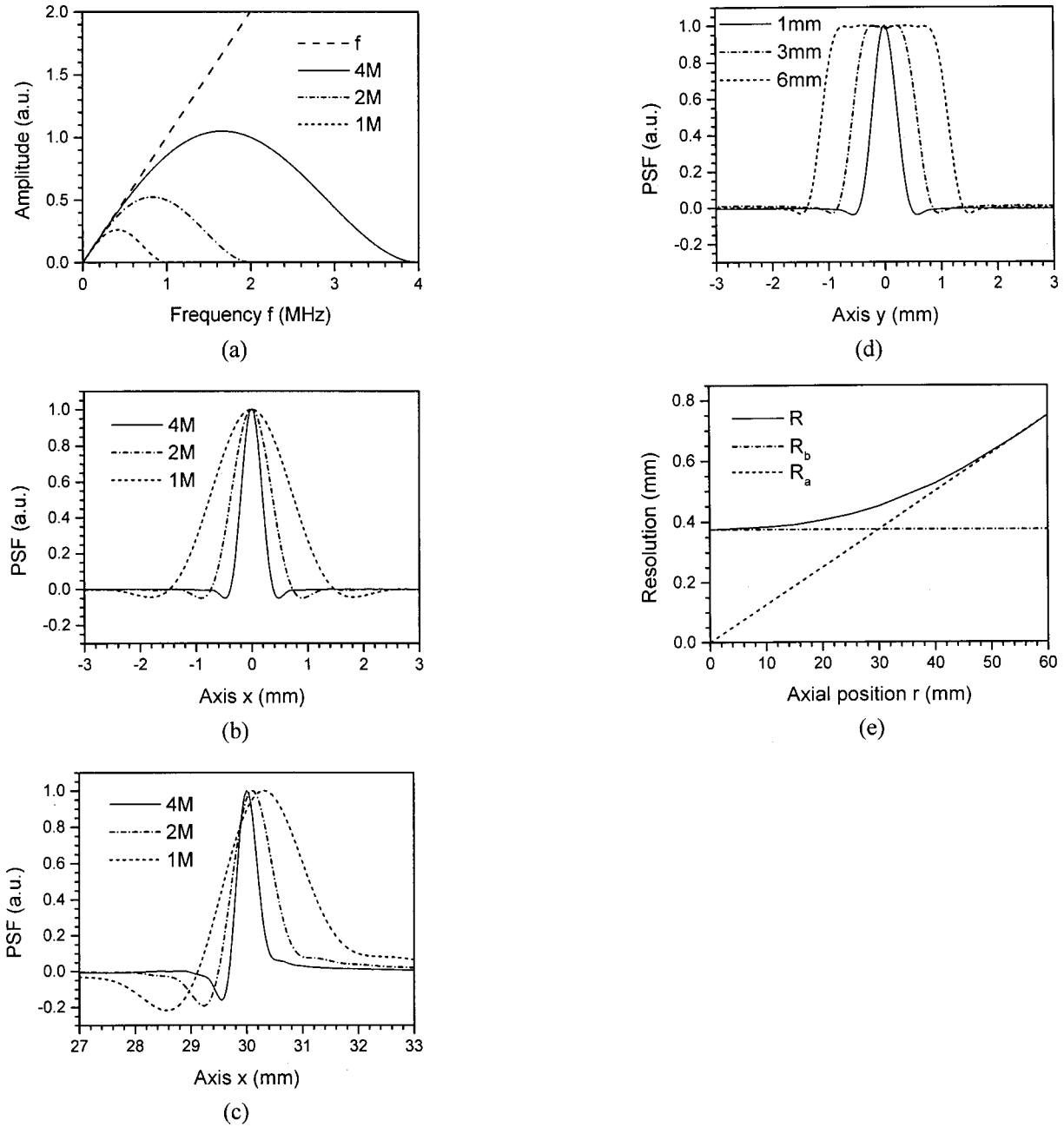


FIG. 5. (a) The pure ramp filter f (dashed line) and the modified filters by Hanning windows with different cutoff frequencies: 4 MHz (solid line), 2 MHz (short dash dotted line) and 1 MHz (short dashed line); Examples of PSF radial profiles with Hanning windows at cutoff frequencies: 4 MHz (solid line), 2 MHz (short dash dotted line) and 1 MHz (short dashed line), when the point source at (b) the origin and (c) the axis $x=30$ mm; (d) examples of PSF profiles in lateral view with different detector aperture size $\delta=1$ mm (solid line), 3 mm (short dash dotted line), and 6 mm (short dashed line), respectively; (e) an example of a comparison with R_a , R_b , and R , where $\delta=1$ mm.

a sufficiently high frequency can restore good spatial resolution and accurate position orientation. Actually, the distortion of the PSF results from the approximation of the FBP algorithm.

For the PSF profiles in Fig. 5(b), the FWHM were measured to be 0.4, 0.9, and 1.5 mm for the cutoff frequencies 4, 2, and 1 MHz, respectively. These values are equivalent to the corresponding half-wavelengths of the central or dominant frequencies of the modified ramp filters: 1.7, 0.8, and 0.4 MHz, respectively. Therefore, the spatial resolution re-

sulting from the bandwidth of the detection system can be estimated by

$$R_b \approx \frac{\lambda_c}{2}, \tag{16}$$

where λ_c is the wavelength of the central or dominant high frequency of the detection system.

In addition to the limitations resulting from the bandwidth of the detection system, the size of the detector aperture is

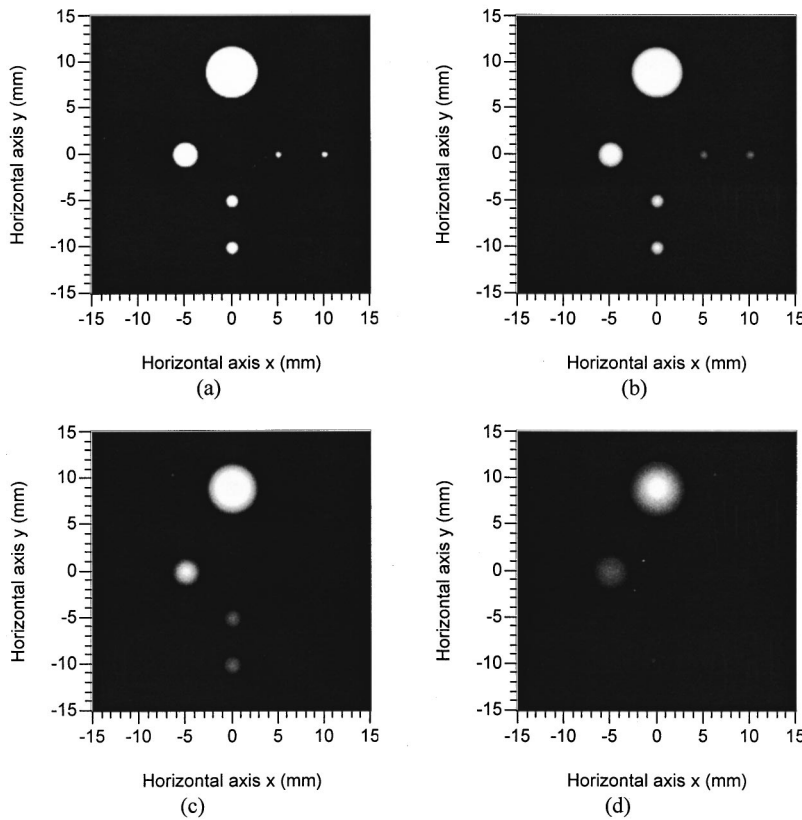


FIG. 6. Examples of reconstructed images with Hanning windows at different cutoff frequencies: (a) 4 MHz, (b) 2 MHz, (c) 1 MHz, and (d) 0.5 MHz respectively.

another factor, which limits spatial resolution. We also chose to investigate its effect through numerical simulation. The received signal in the detector can be simulated by a surface integral divided by its aperture. Then the PSF can be calculated through the FBP, Eq. (4). We assume that the detector has a flat surface with diameter δ .

The simulation demonstrates that the PSF gradually extends along the lateral side but changes very little along the axial direction. Figure 5(d) shows examples of lateral profiles for $\delta=1, 3, \text{ and } 6$ mm, respectively, where the point source at $x_p=30$ mm and $f_\Omega=4$ MHz. It is expected that a big detector aperture will greatly blur the lateral resolution. For convenience, this kind of spatial resolution can be termed R_a , which can be estimated by

$$R_a \approx \frac{r}{r_0} \delta, \quad (17)$$

where r_0 is the radius of the measurement geometry and r is the distance of the point source and the origin. Figure 5(e) shows an example of a comparison with R_a , R_b , and the lateral resolution R , where $\delta=1$ mm; $r_0=80$ mm and $f_\Omega=4$ MHz. Near the origin, $R_a < R_b$, the lateral resolution R is still dominated by R_b . Beyond that where $R_a > R_b$, the lateral resolution R is greatly degraded by the aperture size δ and finally equals R_a . The result also indicates that either a large detector radius r_0 or a small detector aperture δ can improve the lateral resolution in the central region of the detection system. But R_b , i.e., the band limit of the detection system, determines the highest resolution we can obtain.

Let us review the experiment in the previous section. The detector aperture has a 6 mm diameter, and the image region is 30 mm in diameter. Therefore, the worst spatial resolution at $r=30$ mm still has ~ 2 mm. The dominative high frequency of the detection system is about 1.6 MHz, as shown in Fig. 3(b). Thus, the highest resolution is about 0.5 mm. That explains why the word ‘‘OIL’’ in 2 mm diameter can be clearly imaged.

Next, we conduct some numerical experiments. We consider a set of uniform spherical absorbers surrounded by a nonabsorbing background medium. For convenience, we use the centers of the absorbers to denote their positions. We also assume that the pulse duration is very short and can be regarded as a delta function, and, consequently, that the thermoacoustic signal received by the transducer can be calculated by Eq. (3). We employ the circular measurement configuration, as shown in Fig. 1(a). Suppose the circular ultrasonic array consists of 160 elements. The detection radius is 80 mm. There are six spherical absorbers in the $z=0$ plane: a pair of tiny absorbers in diameter 0.75 mm at the positive x axis, a pair of small absorbers in diameter 1.5 mm at the negative y axis, a moderate absorber in diameter 3 mm at the negative x axis, and a big absorber in diameter 6 mm at the positive y axis. Equation (6) is used to compute the filtered thermoacoustic signals with Hanning windows. Figure 6 shows the reconstructed images with different cutoff frequencies: (a) 4 MHz, (b) 2 MHz, (c) 1 MHz, and (d) 0.5 MHz, respectively. As expected, all of the absorbers are clearly imaged, as shown in Fig. 6(a), when the frequency

band is sufficiently wide. However, in the absence of a high-frequency signal, the small size structure is lost. For example, if the cutoff frequency is 1 MHz, the tiny absorbers disappear. For the even lower cutoff frequency of 0.5 MHz, not only do the small absorbers disappear, but also the originally sharp borders of the big absorbers are greatly degraded.

The above numerical simulations gives us clear directions for designing a good image system with \sim mm spatial resolution. The duration of the microwave pulse should be less than 1 μ s, which allows a thermoacoustic signal up to \sim MHz frequency to be generated. The measurement detectors and the preamplifier should have sufficiently wide bands, and the central frequency of the detection system should reach 1–2 MHz. The transducer with a small aperture, such as 1 mm in diameter, is preferred. The small aperture will have less effect on the lateral resolution, and it will reduce the SNR as well. Alternatively, a big detection radius 10–15 cm can be adopted with the sacrifice of signal amplitude because of the acoustic wave propagation attenuation. A wide microwave frequency range from 300 MHz to 3 GHz can be used as the irradiation source. A lower-frequency microwave might be better to image relatively large size samples because it can penetrate deeper.

Finally, we must point out that incomplete measurement data will result in reconstruction artifacts and will degrade the spatial resolution. This topic will be addressed more completely in future work.

VI. CONCLUSION

We have presented our study on pulsed-microwave-induced thermoacoustic tomography in biological tissues by a circular measurement configuration. A filtered backprojection algorithm is used to reconstruct the cross-sectional images. The reconstructed image of a phantom sample agrees with the original values very well. Through numerical simulation, the point-spread function is calculated to estimate the spatial resolution. The results demonstrate that the circular measurement configuration combined with the filtered backprojection method is a promising technique for using microwave absorption contrast and ultrasound spatial resolution (\sim mm) to detect small tumors buried in biological tissues.

ACKNOWLEDGMENTS

This project was sponsored in part by the U.S. Army Medical Research and Materiel Command Grant No. DAMD17-00-1-0455, the National Institutes of Health Grant No. R01 CA71980, the National Science Foundation Grant No. BES-9734491, and Texas Higher Education Coordinating Board Grant No. ARP 000512-0123-1999.

APPENDIX

According to the IEEE standard for safety levels with respect to human exposure to radio frequency electromagnetic fields 3 KHz to 300 GHz (IEEE Std C95.1, 1999 edition), the peak power of maximum permissible exposure (Peak MPE) for a controlled environment in the frequency range f (300–3000 MHz) can be computed by

$$\text{Peak MPE} = \frac{0.24}{N} \times \frac{f}{\text{Pulse width}} \quad (\text{mW/cm}^2),$$

where N is the pulse number per second ($N > 5$) and the pulse width (< 100 ms) is in seconds. In other words, the permissible pulse energy with illumination area S (cm^2) can be estimated by

$$\begin{aligned} \text{Pulse Energy} &= \text{Peak MPE} \times \text{Pulse width} \times S \\ &= \frac{0.24 S f}{N} \quad (\text{mJ}). \end{aligned}$$

In our system, $N = 50$, pulse width = 0.5 ms, and the area of the waveguide $S = 7.2 \times 3.4 \text{ cm}^2 \approx 22 \text{ cm}^2$. Therefore, the permissible pulse energy = $0.24 \times 22 \times 3000 / 50 \approx 300$ mJ. But the pulse energy that we used is only 10 mJ, which is much less than the above permissible value.

Actually, the pulse width is so short that only tiny energy is delivered to the sample. The microwave is not focused and the illumination area is so big that the energy density in the tissue is very low. Suppose the penetration depth of microwave is 1 cm, the energy density E_a due to a pulse microwave excitation can be estimated by

$$\begin{aligned} E_a &= \text{Pulse energy} / (\text{Illumination area } S \times 1 \text{ cm}) \\ &= 10 \text{ mJ} / 22 \text{ cm}^3 \approx 0.45 \text{ mJ/cm}^3. \end{aligned}$$

Then, we can estimate the pressure and temperature rise excited by a pulse microwave in tissue. The muscle contains about 75% water. We take it as an example. In muscle, the volume expansion coefficient is $\beta \approx 3.8 \times 10^{-4} \text{ K}^{-1}$, the heat capacity is $C_p \approx 3.7 \text{ mJ/(g mK)}$, and the mass density is $\rho \approx 1 \text{ g/cm}^3$. Therefore, the Grüneisen parameter = $\beta c^2 / C_p \approx 0.23$, and the generated pressure rise,

$$p = 0.23 \times 0.45 \text{ mJ/cm}^3 \approx 0.1 \text{ mJ/cm}^3 = 1 \text{ mbar},$$

and the temperature rise,

$$\delta T = E_a / (C_p \rho) = 0.45 / 3.7 \approx 0.1 \text{ mK}.$$

As discussed in the paper, the penetration depth in tissue for a microwave below 3 GHz is several centimeters. The Grüneisen parameter in other soft tissue should be close to the value 0.23 in muscle. Therefore, we can conclude that a microwave pulse only causes pressure rise with several millibars and temperature rise with millidegrees. Such tiny values are far beyond causing tissue damage.

^{a)} Author to whom all correspondence should be addressed. Telephone: 979-847-9040; fax: 979-845-4450; electronic mail: LWang@tamu.edu; URL: <http://oilab.tamu.edu>.

¹ R. A. Kruger, K. K. Kopecky, A. M. Aisen, D. R. Reinecke, G. A. Kruger, and W. L. Kiser, "Thermoacoustic CT with radio waves: A medical imaging paradigm," *Radiology* **211**, 275–278 (1999).

² G. Ku and L.-H. V. Wang, "Scanning thermoacoustic tomography in biological tissues," *Med. Phys.* **27**, 1195–1202 (2000).

³ G. Ku and L.-H. V. Wang, "Scanning microwave-induced thermoacoustic tomography: Signal, resolution, and contrast," *Med. Phys.* **28**, 4–10 (2001).

⁴ M.-H. Xu, G. Ku, and L.-H. V. Wang, "Microwave-induced thermoacoustic tomography using multi-sector scanning," *Med. Phys.* **28**, 1958–1963 (2001).

- ⁵R. A. Kruger and P. Liu, "Photoacoustic ultrasound: Pulse production and detection in 0.5% Liposyn," *Med. Phys.* **21**, 1179–1184 (1994).
- ⁶M.-H. Xu and L.-H. V. Wang, "Time-domain reconstruction for thermoacoustic tomography in a spherical geometry," *IEEE Trans. Med. Imaging* (in press). **Update: 21, 814-822, (2002).**
- ⁷M.-H. Xu, Y. Xu, and L.-H. V. Wang, "Thermoacoustic imaging in biological tissues: Time-domain reconstruction algorithms," *IEEE Biomed. Eng.* (submitted).
- ⁸S. Chaudhary, R. Mishra, A. Swarup, and J. Thomas, "Dielectric properties of normal human breast tissues at radiowave and microwave frequencies," *Indian J. Biochem. Biophys.* **21**, 76–79 (1984).
- ⁹W. Joines, Y. Zhang, C. Li, and R. Jirtle, "The measured electrical properties of normal and malignant human tissues from 50–900 MHz," *Med. Phys.* **21**, 547–550 (1994).
- ¹⁰A. C. Tam, "Application of photoacoustic sensing techniques," *Rev. Math. Phys.* **58**, 381–431 (1986).
- ¹¹M. Bertero and P. Boccacci, *Introduction to Inverse Problems in Imaging* (Institute of Physics Publishing, London, 1998).
- ¹²R. A. Kruger, W. L. Kiser, K. D. Miller, H. E. Reynolds, D. R. Reinecke, G. A. Kruger, and P. J. Hofacker, "Thermoacoustic CT: Imaging principles," *Proc. SPIE* **3916**, 150–159 (2000).

Ref. 7 Update: Accepted. □

New title: Time-domain reconstruction algorithms and numerical □
simulations for thermoacoustic tomography in various geometries